Soft Matter

Accepted Manuscript

ROYAL SOCIETY OF CHEMISTRY

www.rsc.org/softmatter

Journal Name

ARTICLE TYPE

Cite this: DOI: 10.1039/xxxxxxxxxx

Probing viscoelastic response of soft material surfaces at the nanoscale†

David B. Haviland*[a], Cornelius Anthony van Eysden[a], Daniel Forchheimer[a], Daniel Platz[a‡], Hailu B. Kassa [b] and Philippe Leclere[b]

Received Date
Accepted Date

DOI: 10.1039/xxxxxxxxxx

www.rsc.org/journalname

We study the interaction between an AFM tip and a soft viscoelastic surface. Using a multifrequency method we measure the amplitude-dependence of the cantilever dynamic force quadratures, which clearly show the effect of finite relaxation time of the viscoelastic surface. A model is introduced which treats the tip and surface as a two-body dynamic problem with a nonlinear interaction depending on their separation. We find good agreement between simulations of this model and experimental data on polymer blend samples for a variety of materials and measurement conditions.

Understanding and controlling forces at the nanometer scale is a scientific problem of importance to a wide variety of technological applications of soft polymer materials[1,2]. Advancement in this field and the development of new nano-materials goes hand-in-hand with ever more sensitive tools and more accurate methods of measuring surface forces. Recent progress in the field of dynamic AFM regarding calibration[3–5] and dynamic methods of force measurement[6–10] has set the stage for a critical examination of the physical models commonly used in describing tip-surface interaction. Meaningful interaction models are crucial to our understanding and interpretation, as they are the link between AFM data and the image or map of a physical property of the material surface.

The mapping of elastic moduli with AFM is usually performed by measuring a dense grid of 'force curves': At each grid point (x,y) the cantilever deflection d is measured as the probe height h is swept toward and away from the surface (see fig. 1). If the cantilever static force constant k_{stat} is calibrated, force is determined from the measured deflection, $F = k_{\mathrm{stat}} d$. Assuming quasi-static force balance, this cantilever force is equal and opposite to the tip-surface force. With an independent measurement of the probe height h one can construct a force curve $F(z)$, showing force as a function of the tip position in the laboratory frame, $z = h + d$. If one can estimate the unperturbed or relaxed position of the surface $z_0(x,y)$ the elastic modulus may be determined by fitting an appropriate model of contact mechanics to this force curve.

Soft materials, like fluids, have the ability to flow and the tip-surface forces can not be described by a purely elastic model. A rheological description of tip-surface interaction should also include entropic forces when the tip penetrates the surface, capillary forces associated with surface curvature, and viscous forces that depend on the velocity of both the tip and the surface[11]. Viscous response has been probed by extending quasi-static AFM to examine force curves at different loading rates (i.e. probe height speed, $\dot{h}$)[12,13]. However, this approach is beset with contradictions: The force-deflection relation $F = k_{\mathrm{stat}} d$ implies quasi-static force balance, yet viscous force requires finite loading rate (i.e. not static). If the measurement is not quasi-static, inertial and viscous forces associated with the motion of the cantilever body must also be properly accounted for.

Understanding viscoelastic response requires a proper analysis of both the cantilever dynamics and the surface dynamics. From the measured cantilever motion we can determine the force acting on the tip. But the AFM does not resolve the motion of the surface and this fact leads to an unappreciated ambiguity in material property mapping with AFM, especially on soft materials. In this paper we show how the independent motion of the tip and surface lead to complex dynamics, which nevertheless can be understood from the amplitude dependence of dynamic force quadratures. We present a new type of dynamic interaction model, where the tip-surface interaction is not expressed as a function of the tip position in the lab frame (i.e. the force curve), but rather as a function for the separation between the moving tip and moving surface. Taking into account surface motion, we are able to model

[a] Nanostructure Physics and Nordita, Royal Institute of Technology (KTH), Roslagstullsbacken 21, SE-10691 Stockholm, Sweden E-mail: haviland@kth.se
[b] Laboratory for Chemistry of Novel Materials, Center for Innovation and Research in Materials and Polymers, University of Mons (UMONS), Place du Parc 20, B-7000 Mons, Belgium

† Electronic Supplementary Information (ESI) available: more detailed description of force quadratures, more complete derivation of the model and additional experimental results. See DOI: 10.1039/b000000x/

‡ Present address: Max Planck Institute for the Physics of Complex Systems, Nöthnitzer Str. 38, 01187 Dresden § Present address: Intermodulation Products AB, Solna, Sweden, intermodulation-products.com

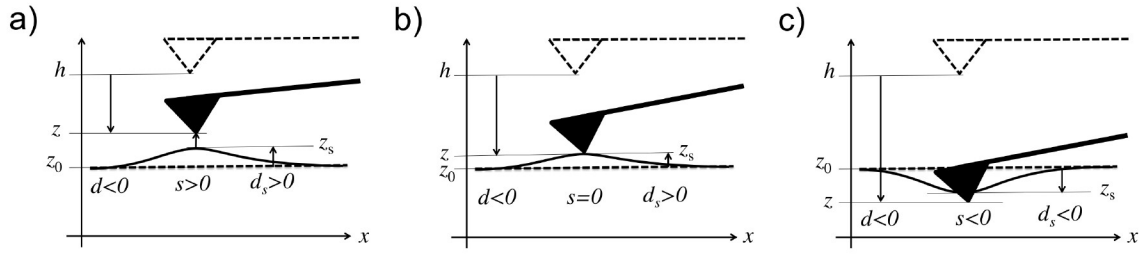

Fig. 1 A sketch (not to scale) demonstrating surface deformation when the tip is a) pulling on, b) contacting, and c) penetrating a soft surface. Coordinates are defined in the intertial reference frame where the bulk of the sample is at rest: h - the quasi-static probe height, controlled by AFM feedback, is the position of the tip when the cantilever force is zero; $d(t)$ - the instantaneous deflection of the tip from the zero-cantilever-force position; $z(t) = h + d(t)$ - the instantaneous position of the tip; $z_0(x,y)$ - the relaxed position of the surface, unperturbed by tip-surface interaction; $z_s(t)$ - the instantaneous position of the surface at the tip location (x,y); and $s(t) = z - z_s = (h - z_0) + d(t) - d_s(t)$ - the instantaneous tip-surface separation.

data measured on soft polymer surfaces and extract the viscous and elastic constants of the surface.

Dynamic AFM typically drives the cantilever at a single frequency where the response phase reveals the energy dissipation experienced by the cantilever[14], but as we shall see below, this dissipation is not directly related to the viscous damping parameter of a soft material surface. Beyond phase imaging, one can measure a grid of response amplitude and phase versus the probe height[15], or with additional feedback, amplitude and frequency shift versus probe height[16]. Viscoelasticity of a surface may also lead to a change in the frequency dependent response of the cantilever[17,18], which is often probed near a contact resonance[19–21], or at two or more frequencies using different cantilever eigenmodes[9,22–24]. A summary of various methods applied to soft materials is given in ref.[25]. An underlying assumption behind many of these methods is that tip-surface forces can be explained from 'rigid contact', with a one-to-one correspondence between tip position and surface deformation.

Here we go beyond linear response and rigid interaction models to explain dynamic AFM data on soft polymer materials. We analyze dynamic force quadratures[10], familiar to polymer scientists from dynamic mechanical analysis[26]. The force quadratures reveal the oscillation amplitude dependence of the forces that are in phase with the harmonic tip motion, and quadrature to the motion, or in phase with the tip velocity. Our analysis shows that significant viscous response can be explained by soft material flow, giving the surface its own dynamics. Our data is well described by a simple model describing a cantilever eigenmode coupled to a linear viscoelastic surface via a nonlinear tip-surface interaction.

Results and discussion

We describe in some detail measurements on a blend of two common polymers, 30% Poly(styrene) (PS) and 70% Poly(ε-caprolactone) (PCL), drop cast from chloroform solution. Results on other blends are given in the supplemental material†. Details of the sample preparation and measurement technique are given in the Methods section. Figure 2 gives an overview of the sample. The central round island is composed of a stiffer material (PS), and it is raised some 750 nm above a surrounding sea of a softer semi-crystalline layered material (PCL). On this PS island, there are many small lakes of an even softer liquid-like material most probably made of amorphous PCL. We determined the mechanical properties of these features with very high spatial resolution in a single scan of duration 8:45 minutes using Intermodulation AFM (ImAFM)[27]. ImAFM drives the cantilever at two frequencies and analyzes the frequency mixing measured at each image pixel (512 x 512).

Figure 3 shows images of the response amplitude and phase at the second drive frequency, one of the 32 image pairs measured in a single scan of ImAFM. With the exception of the response amplitude at the first drive frequency, which is constrained by the AFM feedback used for surface tracking, the amplitude and phase at the two drive frequencies and their 30 measured intermodulation products are free to respond to the complex and highly nonlinear cantilever dynamics. This multifrequency response can be directly transformed into the amplitude-dependent force quadratures $F_I(A)$ and $F_Q(A)$, without any assumptions as to the nature of the tip-surface interaction[10] (see supplemental information†). Figure 3a and 3b show the force quadrature curves at 4 pixels marked with an $\times$ in the corresponding color on the images. Unlike quasi-static force curves, the force quadratures do not represent the force at a particular tip position, $F(z)$, but rather a weighted integral of the tip-surface force over one single oscillation cycle of amplitude A. Each point on the curves in fig. 3 gives the integrated force during a single cycle, as the tip at the lower turning point of the oscillation gradually comes closer to the surface with increasing A, and further from the surface with decreasing A.

If the tip-surface interaction can be expressed as a function of the tip position and velocity alone $F_{TS}(z(t), \dot{z}(t))$, we may interpret F_I as a conservative force (in phase with the cantilever motion) and F_Q a dissipative force (quadrature to the motion, or in phase with the velocity). However this interpretation is not without ambiguity if the interaction depends on other degrees of freedom[7,28], for example the case considered here where F_{TS} depends on the instantaneous separation between a moving tip and independently moving surface.

Positive F_I means that the cantilever experiences a dominantly attractive force during the single oscillation cycle, and negative F_I a dominantly repulsive force. Similarly, negative F_Q corresponds to dissipated energy in the single oscillation cycle of cantilever motion. Apparent in figs. 3a and 3b (especially green and yellow

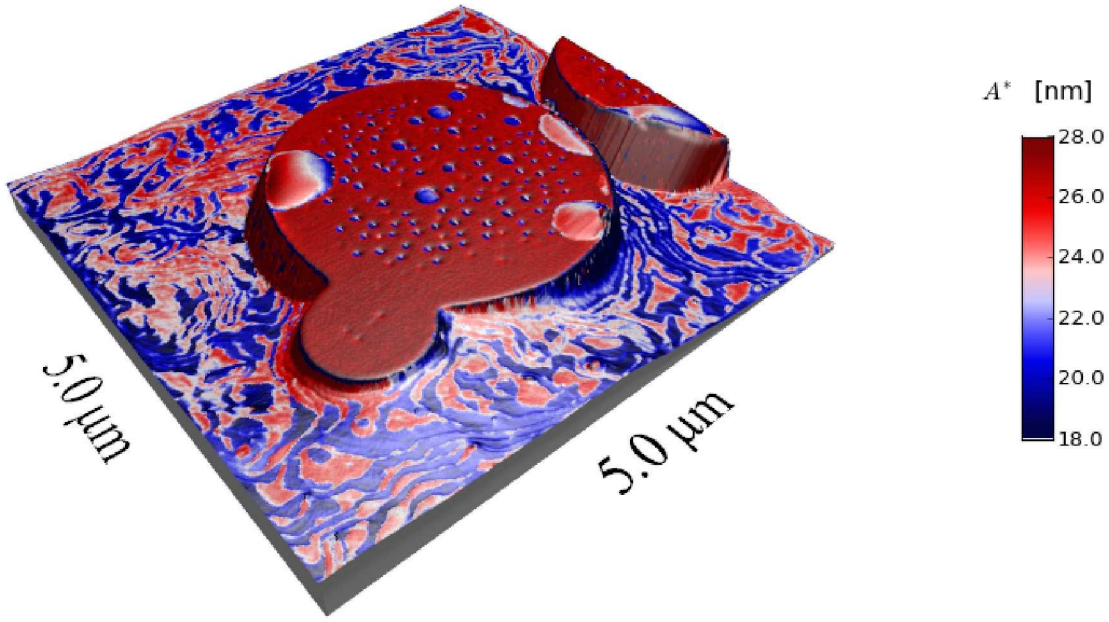

Fig. 2 A three-dimensional perspective of the AFM height data, rendered to scale, where the color codes for the oscillation amplitude A^* at which the conservative force quadrature F_I reaches its maximum value for increasing amplitude.

curves) is the large dissipative force (negative F_Q) in the dominantly attractive regime of conservative force (positive F_I). This observation reveals that before repulsive contact forces set in, attractive forces cause deformation of the soft surface, and due to material flow and viscosity, give rise to dissipation. Hysteresis is also evident in $F_I(A)$ and $F_Q(A)$; a result of the viscoelastic relaxation time of the surface being longer than the period of cantilever oscillation.

Model and simulations

We can explain the various shapes and hysteresis of $F_I(A)$ and $F_Q(A)$ observed with this sample and other soft materials using a simple nonlinear model that includes surface displacement $d_s = z_s - z_0$ as an independent dynamic variable (see fig.1). We consider the surface as having a relaxed position $z_0(x,y)$ (i.e the samples 'true' topography) which, due to material flow during interaction with the tip, can adopt a new instantaneous position $z_s(t;x.y)$. We model the cantilever and surface dynamics with the system of equations (see supplemental information[†]),

$$m\ddot{d} + \eta\dot{d} + kd = F_{ts}(s,\dot{s}) + F_{\rm d}(t) \quad (1)$$

$$\eta_s\dot{d}_s + k_s d_s = -F_{ts}(s,\dot{s}) \quad (2)$$

The left-hand side of Eq. (1) is a good model for the cantilever eigenmode, where all three parameters can be independently calibrated. Eq. (2) reduces the complex three-dimensional surface forces to two parameters, a surface stiffness k_s and surface viscosity η_s respectively. These linear models of the cantilever and surface dynamics are coupled by a nonlinear interaction which is a function of the tip-surface separation $s = z - z_s = (h - z_0) + (d - d_s)$ and its velocity $\dot{s}$, where negative s corresponds to the tip penetrating the surface.

The nonlinear interaction force has two components,

$$F_{ts}(s,\dot{s}) = F_{\rm con}(s) - [\eta_i\dot{s}]_{s<0} \quad (3)$$

For the conservative force $F_{\rm con}(s)$ we use the DMT model[29] (see Methods) to facilitate comparison with other AFM experiments. However, our results thus far are not sensitive to the exact form of $F_{\rm con}(s)$, only that it is characterized by a well-defined point of contact ($s = 0$) with a short-range attraction for $s > 0$ (e.g. van der Waals) and repulsion for $s < 0$ (e.g. local elastic stress). The dissipative part of the interaction is described by the viscosity η_i, which acts only when the tip is penetrating the surface ($s < 0$).

We simulate the dynamics of the system by numerical integration of Eqs. (1) and (2) and from the simulated data we calculate the force quadratures. By adjusting the model parameters (see Table 1) we are able to find remarkably good agreement between the experiment and simulation at essentially any point on the surface. Figures 3c-3h show the simulated results at 4 representative points. The simulation allows us to examine the surface motion, from which we can see that the hysteresis in $F_I(A)$ and $F_Q(A)$ is the result of a finite relaxation time of the viscoelastic surface.

Hysteresis is most pronounced over a very soft area, for example fig. 3h. With increasing amplitude a critical point is reached where short range attractive forces cause a sharp increase to a positive F_I. The attractive interaction pulls up the soft surface and it does not relax before the next oscillation cycle, resulting in a time-average lifted position of the surface. Due to this lifting of the surface, a lower amplitude is required for the tip to stop interacting with the surface, thus giving hysteresis in $F_I(A)$ and $F_Q(A)$.

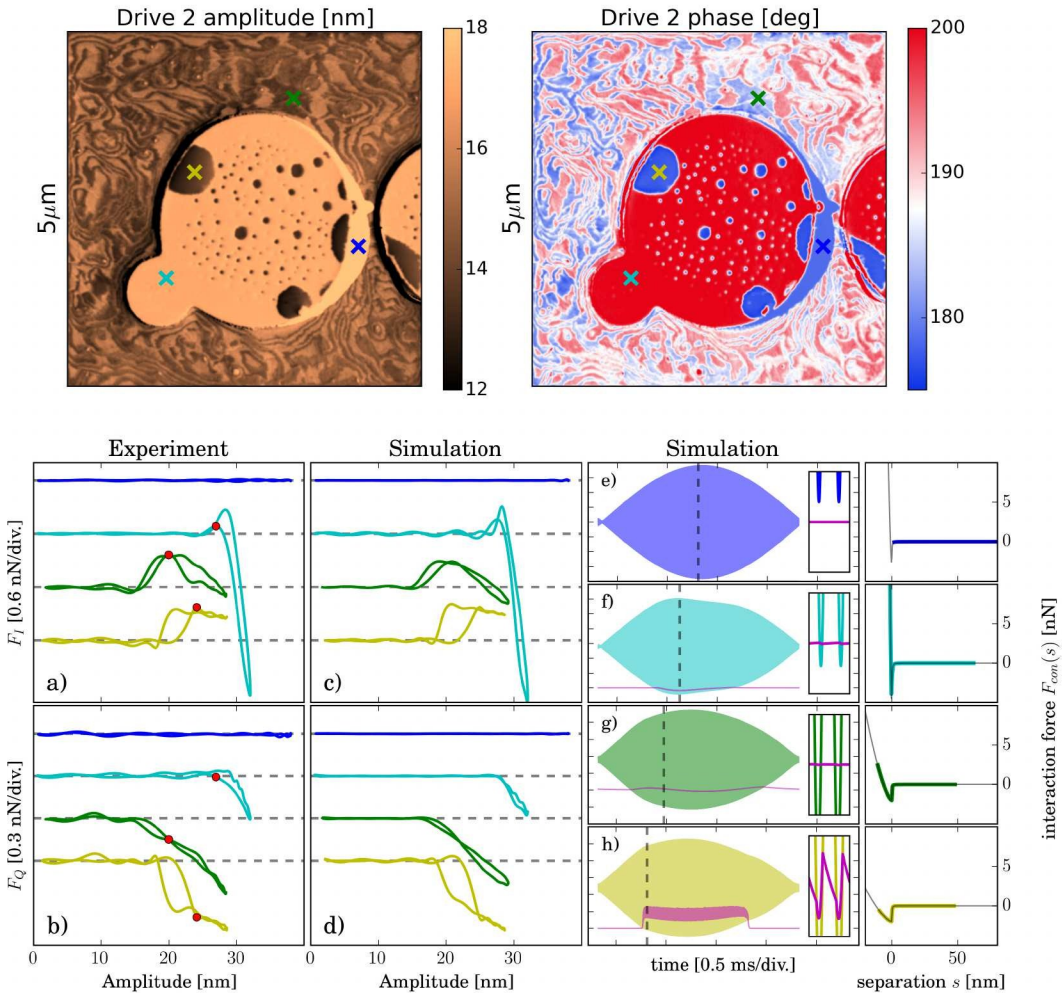

Fig. 3 The amplitude and phase image at the second drive frequency, one of the 32 image pairs recorded during the single scan with ImAFM. a) and b) show experimental $F_I(A)$ and $F_Q(A)$ curves at 4 pixels marked in the images with an $\times$ in the corresponding color. Curves are offset vertically for clarity, where the dashed line indicates zero force. Red dots mark the amplitude A^* where F_I is maximum for increasing amplitude. c) and d) are simulated $F_I(A)$ and $F_Q(A)$ curves using the moving surface model with parameters given in Table 1. e) - h) show the simulated motion of the cantilever (corresponding color) and surface (magenta). The left inset shows the interaction force $F_{ts}(s)$ experienced during the simulated oscillation beat (all left insets have same scale vertical scale -5nN to +10nN). The right inset shows a zoom of the cantilever and surface oscillation in the contact region, at the time marked by the vertical dashed line (all right insets have the same vertical scale spanning 10nm).

Color	surface stiffness k_s [N/m]	surface damping η_s [mg/s]	interaction damping η_i [mg/s]	Reduced Modulus E^* [MPa]	Adhesion Force F_{adh} [nN]	Working distance $h - z_0$ [nm]
cyan	1.000	47	0.71	3500.0	6.0	28.0
green	0.100	28	0.13	40.0	2.0	18.0
yellow	0.050	.24	0.13	15.0	2.0	24.0

Table 1 The model parameter values used for the simulated cures in fig. 3. The DMT model contains two parameters which were fixed for the simulation: the inter-atomic spacing a_0 =0.3 nm and the tip radius R =10nm. The cantilever eigenmode parameters were set to the values measured during calibration: $k = 29.9$ N/m , $Q = k/\eta\omega_0 = 371$, $\omega_0 = \sqrt{k/m} = 2\pi \times 313.57$ kHz. The drive frequencies were set to values used in the experiment: $f_1 = 313.34$ kHz , $f_2 = 313.84$ kHz . Both experimental and simulated $F_I(A)$ and $F_Q(A)$ curves were derived from analysis of 30 intermodulation products measured near resonance.

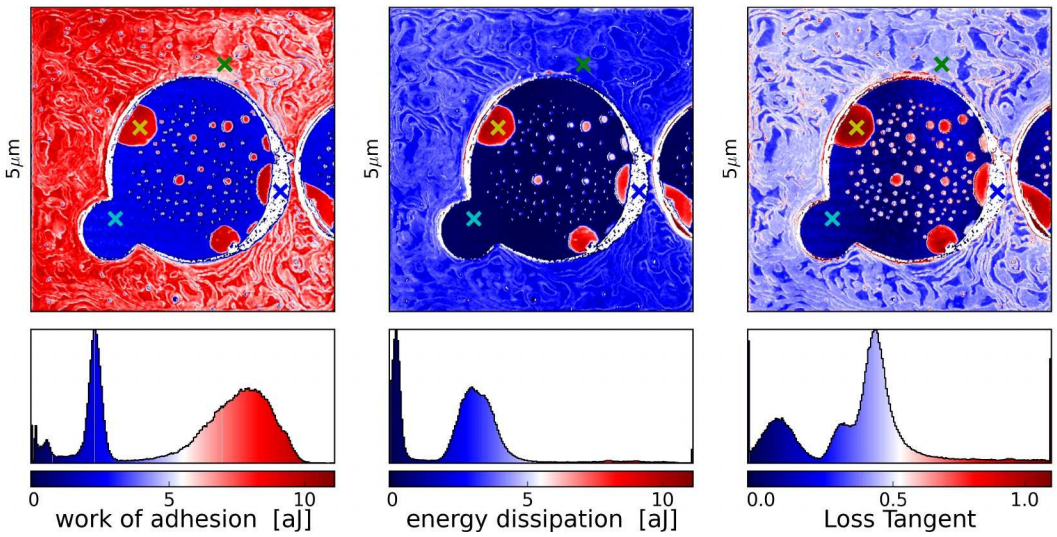

Fig. 4 Maps of the apparent Work of adhesion, Energy Loss and Loss Tangent, as experienced by the oscillating cantilever at the maximum value of $F_I(A)$ for increasing amplitude. These maps compensate for AFM feedback artifacts, but they are nevertheless based on cantilever dynamics at a single oscillation amplitude. Comparison with simulations that include surface motion show that cantilever energy dissipation does not directly reveal the surface damping coefficient.

Work of adhesion and energy dissipation

The simulations reveal the interplay between surface and cantilever dynamics which must be understood if we are to determine surface properties from analysis of cantilever dynamics alone. The situation is further complicated by the AFM feedback used to track the surface, which changes the working distance to the relaxed surface, $h - z_0$, depending on the measured response. We circumvent this latter problem using the amplitude dependence of the force quadratures: We define A^* at every image point as the amplitude at which the conservative force reaches its maximum value $F_{I\max}$ for increasing A (red dots in figs. 3a and 3b). Viewing the force quadrature as a work integral[10], we may define a conserved work of adhesion $W_{\rm adh} = A^* F_{I\max}$ experienced by the cantilever when making and breaking contact with the surface. Similarly, from the dissipative force quadrature at this same amplitude A^* we extract the dissipated energy in this cycle $E_{\rm dis} = A^* F_{Q\max}$. Taking the ratio of the dissipated energy to conserved work, we may also define a loss tangent. We take these values for increasing amplitude as the surface should be minimally effected by excessive penetration or indentation. Note that the amplitude, A^* varies considerably over the surface (see fig. 2).

Figure 4 shows a color-coded map of these experimental quantities. It is interesting to note that the very soft island lakes result in large energy loss of the cantilever, yet they have a much lower surface damping coefficient (yellow ×). The large energy loss is the result of large amplitude of surface motion, induced by the adhesion force $F_{\rm adh}$ pulling on a very soft surface with low stiffness k_s. This example clearly demonstrates the difficulties in directly mapping cantilever forces to surface properties. Because the tip-surface interaction must depend on the tip-surface separation, knowledge of the surface motion is necessary if our goal is to map the material properties k_s and η_s. A fundamental problem with dynamic AFM on soft materials is that our measurement is blind to surface motion. However, through examination of the full amplitude dependence of both dynamic force quadratures and application of this new type of 'two-body' interaction model, we are able to intuit the surface motion.

Conclusion

Dynamic force quadratures reveal the viscoelastic response of the material surface to the point-like load presented by the AFM tip. Measuring the full amplitude dependence of the force quadratures at each pixel allows for removal of artifacts due to the AFM feedback changing the working distance, and it allows us to gain understanding about the surface dynamics. We showed how nanometer scale variations and hysteretic behavior of force quadrature curves can be explained with a new type of interaction model that accounts for movement of the soft surface. With this model we are able to explain measurements on a variety of polymer blends and extract the local viscous and elastic parameters of the heterogeneous surface. The moving-surface model presented here represents a new approach to AFM analysis with the possibility of high resolution mapping of the true surface stiffness and viscosity. Rendering such maps from the multifreqeuncy dynamic AFM data at each pixel will require the application of numerical optimization methods[30] coupled to nonlinear differential solvers.

Methods

Polystyrene (PS) (Mw =18 000 g/mol) was bought from Sigma-Aldrich. The semi-crystalline Poly(ε-caprolactone) (PCL) (Mn= 2000 g/mol) CAPA$^{\rm TM}$ 2200 was purchased from Perstorp. The PS and PCL were dissolved separately in chloroform (10 mg/ml) and a thin film (ca.10 μm) was prepared on a glass substrate from the blend of 30% PS and 70% PCL (in volume) by drop casting, followed by a solvent annealing overnight.

The AFM was a Multimode from Digital Instruments running

on a Nanoscope IIIa controller and version 5 software. Essential to the work present here however was the Intermodulation AFM extension system from Intermodulation Products AB, which can be connected to any host AFM. This system uses a special multifrequency lockin amplifier to excite the cantilever at two frequencies, and monitor the photo-detectors response at many intermodulation products (mixing products) of the two drives. The multifrequency response was analyzed with the quantitative analysis software package from Intermodulation Products AB, which performs the thermal noise calibration of the cantilever (NCHV from Bruker) and the force quadrature analysis. Scanning is controlled by the host AFM which is set to contact mode with the multifrequency lockin supplying the error signal voltage for scanning feedback. Amplitude and phase images at 32 frequencies (64 images in one scan) are collected and displayed in the Intermodulation Products software, which follows the scan by responding to end-of-line and end-of-file trigger signals from the host AFM.

Simulations were made by numerical integration with CVODE, part of the SUNDIALS suite of nonlinear solvers[31]. Discrete event detection was used to ensure that the integrator properly treated the discontinuity in the interaction at $s = 0$. For the conservative part of the interaction we used the DMT model[29],

$$F_{con}(s) = \begin{cases} -F_{\text{adh}} \frac{a_0^2}{(s+a_0)^2} & s > 0 \\ -F_{\text{adh}} + \frac{4}{3} E^* \sqrt{-R s^3} & s < 0 \end{cases} \quad (4)$$

where the reduced modulus E^* is the geometric mean of that for tip and surface, F_{adh} is the adhesion force, R the tip radius (assumed spherical), a_0 is the inter-atomic spacing, and $s = z - z_s$ is the separation between the tip and surface.

Acknowledgments

We gratefully acknowledge financial support from the Olle Engqvist Foundation, the Knut and Alice Wallenberg Foundation, and the Swedish Research Council (VR). C.A.vE was supported by a Nordita fellowship. Ph.L. is FRS-FNRS Senior Research Associate. Research in Mons was supported by the European Commission and Region Wallonne FEDER program, the Science Policy Office of the Belgian Federal Government (BELSPO-PAI VII/5), and the FRS-FNRS PDR Project ECOSTOFLEX.

References

1 Y. Min, M. Akbulut, K. Kristiansen, Y. Golan and J. Israelachvili, *Nat Mater*, 2008, **7**, 527–538.

2 M. A. C. Stuart, W. T. S. Huck, J. Genzer, M. Muller, C. Ober, M. Stamm, G. B. Sukhorukov, I. Szleifer, V. V. Tsukruk, M. Urban, F. Winnik, S. Zauscher, I. Luzinov and S. Minko, *Nat Mater*, 2010, **9**, 101–113.

3 M. J. Higgins, R. Proksch, J. E. Sader, M. Polcik, S. M. Endoo, J. P. Cleveland and S. P. Jarvis, *Review of Scientific Instruments*, 2006, **77**, 013701.

4 J. E. Sader, J. A. Sanelli, B. D. Adamson, J. P. Monty, X. Wei, S. A. Crawford, J. R. Friend, I. Marusic, P. Mulvaney and E. J. Bieske, *Review of Scientific Instruments*, 2012, **83**, 103705.

5 C. A. van Eysden and J. E. Sader, in *Resonant MEMS: Principles, Modeling, Implementation, and Applications*, ed. O. Brand, I. Dufour, S. Heinrich and F. Josse, Wiley-VCH, 2015.

6 F. J. Giessibl, *Phys. Rev. B*, 1997, **56**, 16010.

7 J. E. Sader, T. Uchihashi, M. J. Higgins, A. Farrell, Y. Nakayama and S. P. Jarvis, *Nanotechnology*, 2005, **16**, 94 – 101.

8 M. Stark, R. W. Stark, W. M. Heckl and R. Guckenberger, *PNAS*, 2002, **99**, 8473–8478.

9 O. Sahin, S. Magonov, C. Su, C. F. Quate and O. Solgaard, *Nature Nanotech.*, 2007, **2**, 507.

10 D. Platz, D. Forchheimer, E. A. Tholén and D. B. Haviland, *Nat Commun*, 2013, **4**, 1360.

11 P. de Gennes, F. Brochard-Wyart and D. Quere, *Capillarity and Wetting Phenomena: Drops, Bubbles, Pearls, Waves*, Springer, 2004.

12 M. Radmacher, M. Fritz, C. M. Kacher, J. P. Cleveland and P. K. Hansma, *Biophysical Journal*, 1996, **70**, 556–567.

13 H. Krotil, T. Stifter, H. Waschipky, K. Weishaupt, S. Hild and O. Marti, *Surf. Interface Anal.*, 1999, **27**, 336 –340.

14 J. P. Cleveland, B. Anczykowski, A. E. Schmid and V. B. Elings, *Appl. Phys. Lett.*, 1998, **72**, 2613–2615.

15 E.-C. Spitzner, C. Riesch and R. Magerle, *ACS Nano*, 2011, **5**, 315–320.

16 H. Hölscher, D. Ebeling, J.-E. Schmutz, M. M. Schäefer and B. Anczykowski, in *Scanning Probe Microscopy in Nanoscience and Nanotechnology*, Springer, 2010, pp. 3–21.

17 R. E. Mahaffy, C. K. Shih, F. C. MacKintosh and J. Käs, *Phys. Rev. Lett.*, 2000, **85**, 880–883.

18 N. Yang, K. K. H. Wong, J. R. de Bruyn and J. L. Hutter, *Measurement Science and Technology*, 2009, **20**, 025703.

19 R. Proksch and D. G. Yablon, *Applied Physics Letters*, 2012, **100**, –.

20 D. G. Yablon, A. Gannepalli, R. Proksch, J. Killgore, D. C. Hurley, J. Grabowski and A. H. Tsou, *Macromolecules*, 2012, **45**, 4363–4370.

21 D. C. Hurley, S. E. Campbell, J. P. Killgore, L. M. Cox and Y. Ding, *Macromolecules*, 2013, **46**, 9396–9402.

22 R. Garcia and R. Proksch, *European Polymer Journal*, 2013, **49**, 1897 – 1906.

23 E. T. Herruzo, A. P. Perrino and R. Garcia, *Nat Commun*, 2014, **5**, year.

24 S. D. Solares, *Beilstein Journal of Nanotechnology*, 2014, **5**, 1649–1663.

25 M. Chyasnavichyus, S. L. Young and V. V. Tsukruk, *Japanese Journal of Applied Physics*, 2015, **54**, 08LA02.

26 J. D. Ferry, *Viscoelastic Properties of Polymers*, John Wiley and Sons, 1980.

27 D. Platz, E. A. Tholen, D. Pesen and D. B. Haviland, *Appl. Phys. Lett.*, 2008, **92**, 153106–1.

28 U. Dürig, *New Journal of Physics*, 2000, **2**, year.

29 B. V. Derjaguin, V. M. Muller and Y. P. Toporov, *Journal of Colloid and Interface Science*, 1975, **53**, 314.

30 D. Forchheimer, D. Platz, E. A. Tholén and D. B. Haviland,

Phys. Rev. B, 2012, **85**, 195449.

31 A. C. Hindmarsh, P. N. Brown, K. E. Grant, S. L. Lee, R. Serban, D. E. Shumaker and C. S. W. ACM, *Transactions on Mathematical Software*, 2005, **31**, 363–396.

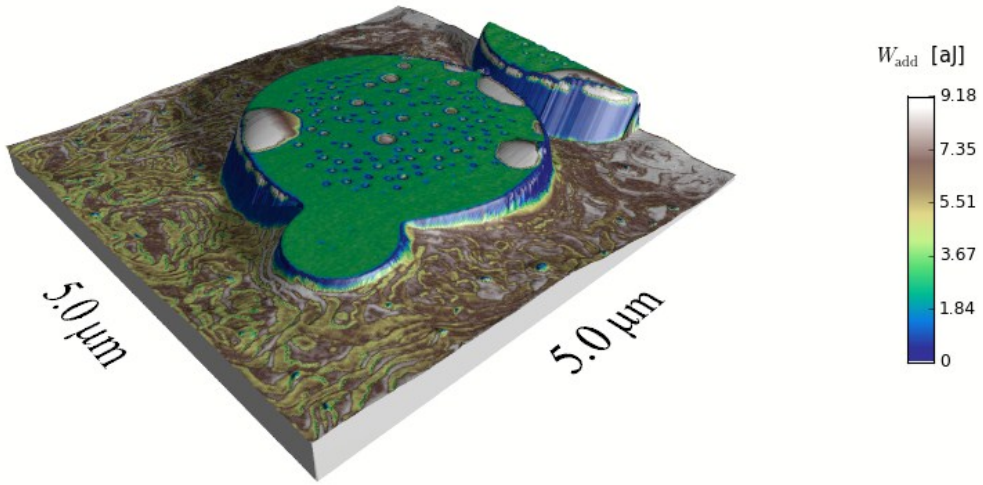

Intermodulation Atomic Force microscopy is used to quantitatively determine both viscous and elastic parameters of a soft material interface. To understand the measured force quadratures at each image pixel, a dynamic model of the tip surface interaction is introduced, taking in to account not only the dynamics of the AFM cantilever, but also the dynamics of the viscoelastic surface.